Title
Quantification of a three-dimensional velocity vector using spectral-domain Doppler optical coherence tomography.

Journal
Optics Letters, 32(11)

ISSN
0146-9592

Authors
Ahn, Yeh-Chan
Jung, Woonggyu
Chen, Zhongping

Publication Date
2007-06-01

DOI
10.1364/ol.32.001587

Quantification of a three-dimensional velocity vector using spectral-domain Doppler optical coherence tomography

Yeh-Chan Ahn, Woonggyu Jung, and Zhongping Chen*

Beckman Laser Institute and Department of Biomedical Engineering, University of California, Irvine, Irvine, California 92617, USA

**Corresponding author: z2chen@uci.edu*

Received February 23, 2007; accepted March 26, 2007;
posted April 9, 2007 (Doc. ID 80374); published May 18, 2007

Multiangle, fiber-based, spectral-domain Doppler optical coherence tomography with a phase-resolved algorithm is presented to measure three components of an arbitrary velocity vector. A beam divider that divides a probe beam to have five independent viewpoints and path length delays was designed. The divider was inserted into the sampling arm of a Doppler optical coherence tomography system between the collimator and the first galvo mirror of a two-axis galvo scanner. The divider produced five independent $\Delta\mathbf{k}$'s (the average difference between the wave vectors of incoming and outgoing beams) after passing through the focusing lens while keeping two-axis scanning capability. After calibration, an unknown velocity vector field inside a microtube was quantified by solving a three-dimensional minimization problem. © 2007 Optical Society of America

OCIS codes: 170.4500, 170.3890.

As applications of the biofluidic chip become more diverse, the geometry of the chip becomes more complex, and the flow field inside the biofluidic chip has been changed from a simple Poiseuille flow to three-dimensional fields. The complex nature of the biofluidic chip requires a novel probe that acts like the scanning electron microscope in the semiconductor industry and assures quality control by diagnosing structure and flow in real time and noninvasively. Since Doppler optical coherence tomography (DOCT) was developed [1,2], it has been used to quantify the structure and flow in microchannels [3,4]. Conventional DOCT, however, has a low-velocity dynamic range and a limitation that only the component of the velocity parallel to the optical axis can be measured. Spectral-domain DOCT developed recently has a higher-velocity dynamic range than conventional DOCT. Multiangle and Doppler variance imaging techniques have been tried to measure transversal velocity [5–11]. However, three components of a velocity vector have not yet been measured with fiber-based DOCT. Microparticle imaging velocimetry (micro-PIV) [12,13] is a powerful tool for imaging microscale flows. However, micro-PIV does not work with a turbid biofluid such as blood. In addition, it is difficult for micro-PIV to quantify out-of-plane velocities that are parallel to an incident light [14].

From the relationship between Doppler shift Δf and velocity vector $\mathbf{V}$, at least three independent $\Delta\mathbf{k}$ vectors are necessary to represent the velocity vector:

$$\Delta f_i = \Delta\phi_i/2\pi T = \mathbf{V}\cdot\Delta\mathbf{k}_i/2\pi \qquad (i = 1,2,3,\ldots), \quad (1)$$

where $\Delta\phi$ is the phase difference of two complex signals acquired from the inverse Fourier transform of spectra taken by two camera exposures, T is the time interval between the two exposures, and $\Delta\mathbf{k}$ denotes the difference between the intensity-weighted, area-averaged wave vectors of incoming and outgoing beams, $\Delta\mathbf{k}=(\mathbf{k}_{out}-\mathbf{k}_{in})$. To measure at least three Doppler shifts with one detector (or spectrometer), each beam path associated with a different $\Delta\mathbf{k}$ should have a different time of flight.

In this study, we propose a multiangle, fiber-based, spectral-domain DOCT with a beam divider that divides a probe beam to have five independent $\Delta\mathbf{k}$'s with five different path length delays. Figure 1(a) shows the beam divider. It has three parts (A, B, and C) with different thicknesses (0, t, and $2t$) and is inserted into the sampling arm of a fiber-based, spectral-domain DOCT system between the collimator and the first galvo mirror of a two-axis galvo scanner as shown in Fig. 2. In the subscript of $\Delta\mathbf{k}$ in Fig. 1, the first two letters indicate through which part of the divider the incoming and outgoing beams go. For instance, $\Delta\mathbf{k}_{AB}$ means that the incoming beam passes

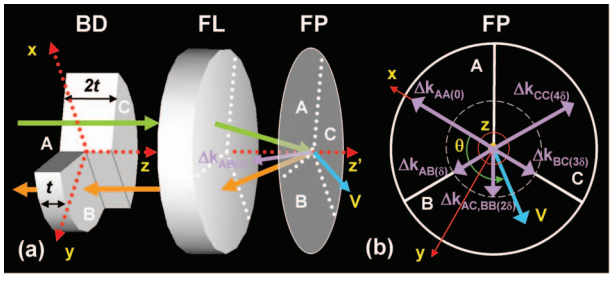

Fig. 1. The three parts (A, B and C) of the developed beam divider make six different beam paths: AA, BB, CC, AB, BC, and AC. Each path generates one $\Delta\mathbf{k}$ and experiences different path length delays (shown in parentheses) because the three parts have different thicknesses. Since $\Delta\mathbf{k}_{AC}$ and $\Delta\mathbf{k}_{BB}$ have a same path length delay of 2δ, there are five independent $\Delta\mathbf{k}$'s with five different path length delays. Panel (a) shows how $\Delta\mathbf{k}_{AB}$ is produced. Panel (b) depicts $\Delta\mathbf{k}$'s and an arbitrary velocity vector $\mathbf{V}$ when one sees them along the z axis. BD, beam divider; FL, focusing lens; FP, focal plane.

0146-9592/07/111587-3/$15.00

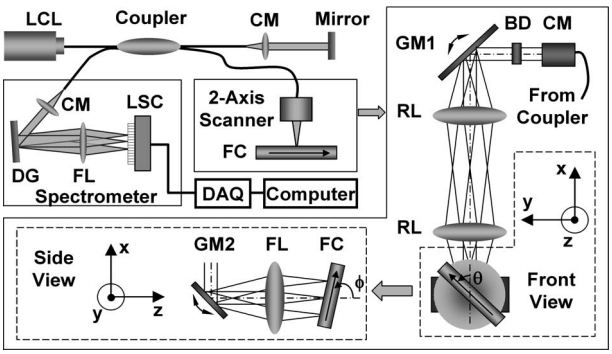

Fig. 2. Schematic of fiber-based, spectral-domain DOCT: a 130 nm wide spectrum was sampled by a 1×1024 InGaAs detector array at 7.7 kHz. Imaging depth and depth resolution were 3.4 mm and 8 μm in air, respectively. A two-axis scanner with two galvo mirrors was used. A microtube with a 300 μm inner diameter was rotated by θ in the xy plane from the x axis and ϕ from the z axis. BD, beam divider; CM, collimator; DAQ, data acquisition system; DG, diffraction grating; FC, flow channel; FL, focusing lens; GM, galvo mirror; LCL, low-coherence light; LSC, line scan camera; RL, relay lens.

through part A and the outgoing beam through part B or vice versa. In the parentheses, the relative optical path length delay is included. Instead of the long subscript, the index i is also used hereafter and increases with the order of path length delay.

The three parts of the beam divider make six different beam paths: AA, BB, CC, AB, BC, and AC. Each path generates one $\Delta\mathbf{k}$ and experiences different path length delays because the three parts have different thicknesses. Since the $\Delta\mathbf{k}_{AC}$ and $\Delta\mathbf{k}_{BB}$ have the same path length delay of 2δ, there are five independent $\Delta\mathbf{k}$'s with five different path length delays. The z axis in Figs. 1(a) and 2 does not represent the optical axis of the focusing lens (denoted z') but the axis of the scanning beam after the focusing lens. Figure 1(a) shows how $\Delta\mathbf{k}_{AB}$ is produced for the case when the z and z' axes are collinear. Eventually, the beam divider produces five different points of view toward a sample after passing through the focusing lens while keeping two-axis scanning capability. Figure 1(b) shows $\Delta\mathbf{k}$'s and an arbitrary velocity vector $\mathbf{V}$ when one sees them along the z axis.

Assuming that the refractive index of the divider is n, δ is equal to $t(n-1)$, and two neighboring Doppler images have a shift of $\delta/2$ in the A-scan direction. The maximum imaging depth in optical length is equal to $N\lambda^2/4\Delta\lambda$ for spectrometer-based, spectral-domain DOCT, where N is the number of the detector array in the camera, λ is the center wavelength of the light source, and $\Delta\lambda$ is the full spectral range of the spectrometer. If one wants to see all five Doppler images, the thickness t should, at most, be $N\lambda^2/10\Delta\lambda(n-1)$. The $\delta/2$ image shift is, then, $N\lambda^2/20\Delta\lambda$. Hence an image with an optical depth larger than $N\lambda^2/20\Delta\lambda$ will overlap with its neighbor.

The schematic of fiber-based, spectral-domain DOCT with 8 μm (in air) depth resolution is shown in Fig. 2. Low-coherence light having a 1310 nm center wavelength with a full width at half-maximum bandwidth of 95 nm was coupled into the source arm of a fiber-based Michelson interferometer. Backreflected lights from the reference and sample arms were guided into a spectrometer. The dispersed spectrum was sampled by the spectrometer with a 1×1024 InGaAs detector array at 7.7 kHz. The wavelength range on the array was 130 nm, corresponding to a spectral resolution of 0.13 nm and an imaging depth of 3.4 mm in air. The probe beam divided by the beam divider had a 15 μm spot at the focal point and was scanned by a two-axis scanner to visualize a flow inside a microtube. The two-axis scanner consisted of a collimator, a beam divider, two galvo mirrors, two relay lenses, and a focusing lens. A beam divider with $t=3.0$ mm was made of glass. The spectral-domain DOCT was operated with phase-resolved algorithm. The microtube with an inner diameter of 300 μm was rotated by θ in the xy plane from the x axis and ϕ from the z axis; θ and ϕ are the azimuthal angle with $0\leqslant\theta<2\pi$ and the polar angle with $0\leqslant\phi\leqslant\pi$, respectively. The polar and azimuthal angles were controlled by a goniometer and a rotational stage, respectively. An aqueous solution of polystyrene beads was injected into the microtube. Flow inside the microtube was imaged with the five independent $\Delta\mathbf{k}$'s as a function of θ, ϕ, and velocity magnitude V.

Doppler shifts in Eq. (1) can be represented in spherical coordinates:

$$\Delta f_i = V[A_i \sin\phi\cos(\theta - B_i) - C_i\cos\phi] \qquad (i=1\ldots5), \tag{2}$$

where

$$A_1 = 2A_2 = 2A_3 = 2A_4 = A_5 = 2k\sin\alpha/\pi,$$

$$B_i = \pi(i-1)/3,$$

$$C_1 = C_2 = C_3/2 = C_4 = C_5 = 2k\cos\alpha/\pi.$$

Here α is an effective numerical aperture of the focusing beam to be calibrated experimentally, and k denotes the magnitude of the wave vector. The second term in Eq. (2) is a contribution of the velocity component parallel to the z axis.

Since it is difficult to measure actual $\Delta\mathbf{k}$'s directly, those were represented as in Eq. (2) with unknown coefficients A_i, B_i, and C_i and identified indirectly from known velocity vectors and measured Δf's. Forty known velocity vectors for $\theta=0°-360°$ and $\phi=80°-100°$ were selected. The Δf's were measured for each known velocity vector. Figure 3 shows the calibration results. By design the $\Delta\mathbf{k}_{AC}$ and $\Delta\mathbf{k}_{BB}$ should represent the same path length delay of 2δ. In reality, the thickness of area C was not exactly $2t$, so that the third image, related to Δf_3, was unsatisfactory and therefore discarded.

Once the calibration was done, an arbitrary velocity vector $\mathbf{V}$ could be determined by using Fig. 3. To identify the velocity vector $\mathbf{V}$, we defined an error estimator

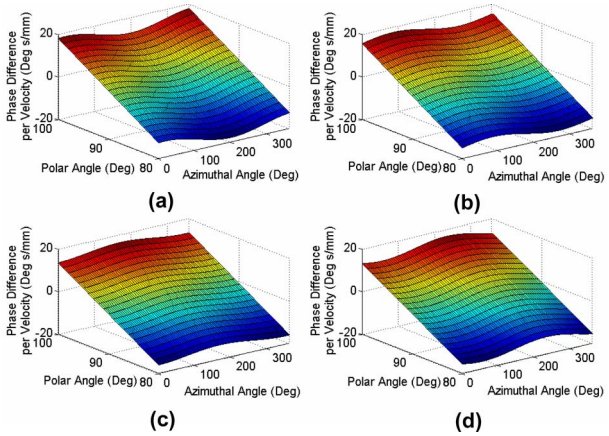

Fig. 3. (Color online) Calibration results for (a) Δf_1, (b) Δf_2, (c) Δf_4, (d) Δf_5.

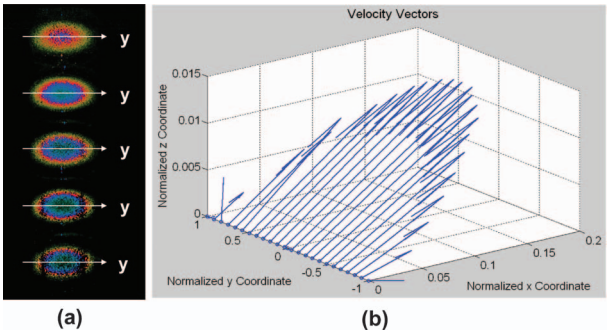

Fig. 4. Velocity vector field measured by the spectral-domain DOCT along the diameter of the microtube. Velocity vectors (b) were identified from the five Doppler images (a) of a cross section.

$$\|\widetilde{\Delta f_i} - \mathbf{V}\cdot\Delta\widetilde{\mathbf{k}}_i/2\pi\| \qquad (i=1,2,4,5), \tag{3}$$

where $\widetilde{\Delta f_i}$ is a Doppler shift fitted over a cross section and $\widetilde{\Delta\mathbf{k}_i}$ is the actual $\Delta\mathbf{k}_i$ that is represented in terms of A_i, B_i, and C_i. A genetic algorithm was used to minimize the error estimator with three unknowns of V, θ, and ϕ. Figure 4(a) shows five Doppler images of the microtube with an unknown flow rate and orientation. The three-dimensional minimization problem was solved, and the result is depicted in Fig. 4(b). The velocity vector field had a parabolic profile. The spatial coordinates were normalized with the radius of the microtube. The velocity vector at the center of the microtube had $V=37.85$ mm/s, $\theta=0°$, and $\phi=85.2°$. We also read the flow rate from a syringe pump and the orientation from the goniometer and rotational stage. The readings were $V=38.73$ mm/s, $\theta=0°$, and $\phi=82.6°$. The two results had good agreement with each other. If we chose evenly 90 velocity vectors within a half of the diameter around the center, the standard deviations of θ and ϕ were 1.97° and 0.32°, respectively.

In summary, we have developed multiangle, fiber-based, spectral-domain Doppler optical coherence tomography to quantify an unknown velocity vector field. We proposed a beam divider that makes five independent $\Delta\mathbf{k}$'s and path length delays. A velocity vector field in a microtube was quantified with good accuracy.

We thank Jeehyun Kim and J. Stuart Nelson for their help. This work was supported by the National Science Foundation (BES-86924), National Institutes of Health (EB-00293, NCI-91717, RR-01192), and the Air Force Office of Science Research (FA9550-04-1-0101). Institutional support from the Beckman Laser Institute Endowment is also gratefully acknowledged.

References

1. Z. Chen, T. E. Milner, D. Dave, and J. S. Nelson, Opt. Lett. **22**, 64 (1997).
2. J. A. Izatt, M. D. Kulkarni, S. Yazdanfar, J. K. Barton, and A. J. Welch, Opt. Lett. **22**, 1439 (1997).
3. Y.-C. Ahn, W. Jung, and Z. Chen, Appl. Phys. Lett. **89**, 064109 (2006).
4. Y.-C. Ahn, W. Jung, J. Zhang, and Z. Chen, Opt. Express **13**, 8164 (2005).
5. Y. Zhao, Z. Chen, C. Saxer, Q. Shen, S. Xiang, J. F. de Boer, and J. S. Nelson, Opt. Lett. **25**, 1358 (2000).
6. H. Ren, K. M. Brecke, A. Ding, Y. Zhau, J. S. Nelson, and Z. Chen, Opt. Lett. **27**, 409 (2002).
7. D. P. Davé and T. E. Milner, Opt. Lett. **25**, 1523 (2000).
8. L. Wu, Opt. Lasers Eng. **42**, 303 (2004).
9. C. J. Pedersen, D. Huang, M. A. Shure, and A. M. Rollins, Opt. Lett. **32**, 506 (2007).
10. H. Yokoyama, M. Akiba, K. P. Chan, and N. Tanno, in *Conference on Laser and Electro-Optics Technical Digest, CLEO/Pacific Rim 2001, 4th Pacific Rim Conference on Laser and Electro-Optics* (2001), paper TuD1-5.
11. A. Røyset, T. Støren, F. Stabo-Eeg, and T. Lindmo, Proc. SPIE **6079**, 607925 (2006).
12. C. D. Meinhart, S. T. Wereley, and J. G. Santiago, Exp. Fluids **27**, 414 (1999).
13. J. G. Santiago, S. T. Wereley, C. D. Meinhart, D. J. Beebe, and R. J. Adrian, Exp. Fluids **25**, 316 (1998).
14. F. Pereira and M. Gharib, Meas. Sci. Technol. **13**, 683 (2002).